Canonical variational transition-state theory study of the CF 3CHFCH2F + OH reaction

ARTICLE *in* THE JOURNAL OF PHYSICAL CHEMISTRY A · FEBRUARY 2010

Impact Factor: 2.69 · DOI: 10.1021/jp909675u · Source: PubMed

4 AUTHORS, INCLUDING:

Angels Gonzalez-Lafont
Autonomous University of Barcelona
119 PUBLICATIONS **1,992** CITATIONS
SEE PROFILE

José M Lluch
Autonomous University of Barcelona
270 PUBLICATIONS **4,266** CITATIONS
SEE PROFILE

Adrián Varela-Álvarez
AstraZeneca
22 PUBLICATIONS **385** CITATIONS
SEE PROFILE

Canonical Variational Transition-State Theory Study of the CF_3CHFCH_2F + OH Reaction

Àngels González-Lafont,*,† José M. Lluch,† Adrián Varela-Álvarez,‡ and José A. Sordo‡

Departament de Química, Universitat Autònoma de Barcelona, 08193 Bellaterra, Barcelona, Spain and Laboratorio de Química Computacional, Departamento de Química Física y Analítica, Universidad de Oviedo, 33006 Oviedo, Principado de Asturias, Spain

Received: October 9, 2009; Revised Manuscript Received: January 25, 2010

Variational transition-state theory rate constants with multidimensional tunneling contributions using the small curvature method have been calculated for the CF_3CHFCH_2F (HFC-245eb) + OH reaction over a temperature range from 200 to 800 K. The mPW1B95−41.0 hybrid functional, parametrized by Albu and Swaminathan to generate theoretical rate constants nearly identical to the experimental values for the CH_3F + OH reaction, has been used in conjunction with the 6-31+G(d,p) basis set to explore the potential energy surface of the title reaction. The functional provides results within the limits of chemical accuracy, supporting the conclusions about transferability of a previous study on the $CF_3CH_2CH_3$ + OH reaction. Fourteen different reaction channels have been explored, all of them with significant contributions to the global rate constants.

Introduction

For a number of years chlorofluorocarbons (CFCs) were widely used in industrial and housewares applications. This family of compounds presents two major inconveniences:[1,2] (1) CFCs are a source of chlorine in the stratosphere, which is a main cause of ozone depletion; and (2) CFCs are greenhouse gases due to the C−Cl and C−F bonds.

Hydrofluorocarbons (HFCs) have been proposed as alternative for CFCs. The absence of chlorine and bromine in HFCs composition makes this family of compounds more ozone-friendly. Nevertheless, HCFs still contribute to global warming because of the presence of C−F bonds. This last flaw is not as severe as for CFCs because HFCs have shorter lifetimes than CFCs, that is, HFCs are degraded by hydroxyl (OH) radicals.[2]

The starting reaction of the HFCs degradation is a hydrogen abstraction process by OH radical. Obviously, the faster this reaction for a given HFC, the more suitable the HFC is as a substitute for CFCs. A great number of experimental studies have been carried out to assess the goodness of different HFCs.[3−7] In particular, two articles present results for the reaction of CF_3CHFCH_2F (HFC-245eb) with the hydroxyl radical:[6,7]

(1) Nelson and co-workers[6] used a discharge flow technique with laser-induced fluorescence detection (DF-LIF) on OH radicals in order to obtain a rate constant at 298 K. A value of $k_{exp}^{Nel} = (1.48 \pm 0.17) \times 10^{-14} cm^3 \cdot molecule^{-1} \cdot s^{-1}$ is reported for the rate constant.

(2) Recently, Ravishankara and co-workers[7] used pulsed laser photolysis with laser-induced fluorescence detection (PLP-LIF) of the OH radicals. The measurements were carried out between 238 and 374 K, and a nonweighted linear least-squares fit of the corresponding Arrhenius plot yielded:

$$k_{exp}^{Rav}(T) = (1.23 \pm 0.18) \times 10^{-12} \exp[(-1250 \pm 40)/T] \quad cm^3 \cdot molecule^{-1} \cdot s^{-1}$$

Using this equation at 298 K gives:

$$k_{exp}^{Rav}(298K) = (1.81 \pm 0.18) \times 10^{-14} \, cm^3 \cdot molecule^{-1} \cdot s^{-1}$$

which is a value slightly higher than the one reported by Nelson and co-workers.

Nowadays, none of the available experimental techniques can be considered routine or low-cost. As a consequence, a few authors,[4,5,8,9] mainly Atkinson and co-workers, used the available experimental information on the rates of several reactions to obtain empirical equations that could predict the rate constants for reactions of OH radical with species of particular interest. Although the original general structure activity relationship (SAR) developed by Atkinson and co-workers fails for HFCs,[8] a number of modifications have been proposed and other empirical methods have been developed.[4,5,9] Additionally, several authors have developed correlations between kinetics parameters of those OH radical reactions and the molecular parameters of HFCs.[10−12]

Ravishankara and co-workers[7] applied the SAR method derived by Tokuhashi and co-workers[9] and the one developed by DeMore[4] to the title reaction. They found that both methods predict an equal contribution of the CHF and CH_2F groups to the global rate constant.

HFCs have also attracted a lot of attention from the theoretical chemistry community. Most of the publications deal with fluorometanes and fluoroetanes,[13−25] but examples of fluoropropanes are also present through scientific literature.[26−28] Nowadays, theoretical studies can provide quite accurate numerical values of gas-phase rate constants, which can then be employed, along with the experimental results, to obtain rate constants as reliable as possible to be used in atmospheric investigations. The main advantage of the theoretical kinetics studies is perhaps that they offer very useful and detailed information at the molecular level of the reaction mechanisms.

* To whom correspondence should be addressed. E-mail: angels@klingon.uab.es.
† Universitat Autònoma de Barcelona.
‡ Universidad de Oviedo.

10.1021/jp909675u
Published on Web 02/09/2010

This information is usually unavailable for the current experimental methods. In this sense, the present theoretical article aims at getting a deeper insight into the mechanism of the title reaction, intending to identify and weight all the factors and channels that overall determine the global rate constant. At this point it is worth noting that the studied chemical process actually involves two reactions, because the secondary hydrogen as well as the primary hydrogens can be abstracted by the OH radical:

$$CF_3CHFCH_2F + OH \rightarrow CF_3CFCH_2F + H_2O \quad \text{(R1)}$$

$$CF_3CHFCH_2F + OH \rightarrow CF_3CHFCHF + H_2O \quad \text{(R2)}$$

On the other hand, very recently Albu and Swaminathan[24] have adjusted the percentage of the exact exchange of a hybrid meta-GGA density functional in order to improve the description of the kinetics of the $CH_3F + OH$ reaction. On a previous work[27] we have shown the goodness of the transferability of this functional for the $CF_3CH_2CH_3 + OH$ reaction. It is clear that more examples are necessary to assess if this was a fortuitous good result or if that functional is actually transferable from CH_3F to any member of the HFCs family. Thus, the results presented in this paper will allow us to further check the hypothesis of transferability.

While this paper was being written, a partial theoretical study of the $CF_3CHFCH_2F + OH$ reaction by Gao et al.[28] was published. In that work only the contributions from the most stable conformer of CF_3CHFCH_2F were considered, in such a way that less than one-third (4 transition state structures) of the possible channels leading from reactants to products were included in their calculations. In the present paper we have calculated the variational transition-state theory rate constants with multidimensional tunneling contributions for the title reaction, including, for the first time, all the reaction channels (14 transition state structures) playing a role in the reaction, thus providing a comprehensive view of the mechanism.

Method of Calculation

Electronic Structure Calculations. All electronic structure calculations were carried out using the Gaussian 03 suite of programs.[29] A very tight criterion for the SCF convergence and a very dense grid (99 spheres of 974 points) were used. Also a tight criterion was used for all the optimizations.

The nature of the located stationary points was characterized according to the number of imaginary vibrational frequencies. The mPW1B95−41.0[24a,30,31] hybrid meta-GGA[32] density functional in conjunction with the 6-31+G(d,p) basis set was used. This functional has an amount of Hartree−Fock exchange (41%) adjusted by Albu and Swaminathan using the model reaction:[24a]

$$CH_3F + OH \rightarrow CH_2F + H_2O$$

This functional was used previously to study the reactions:[27]

$$CF_3CH_2CH_3 + OH \rightarrow CF_3CH_2CH_2 + H_2O$$

$$CF_3CH_2CH_3 + OH \rightarrow CF_3CHCH_3 + H_2O$$

showing a promising performance.

TABLE 1: Classical Potential Energy (ΔV), Adiabatic Potential Energy (ΔV_a^G), Enthalpy ($\Delta H°$ (298 K)), Entropy ($\Delta S°$ (298 K, 1 M)), and Free Energy ($\Delta G°$ (298 K, 1 M)) for the Reaction R1[a]

structure	ΔV	ΔV_a^G	$\Delta H°$	$\Delta S°$	$\Delta G°$
RA	0.0	0.0	0.0	0.0	0.0
RB	1.1	1.1	1.1	0.6	0.9
RC	1.2	1.4	1.3	−1.1	1.6
TS_RA-RB	1.8	1.7	1.2	−4.1	2.4
TS_RB-RC	4.8	4.8	4.3	−5.5	5.9
TS_RA-RC	5.9	6.0	5.5	−4.4	6.8
pre_TSAa1	−3.5	−2.6	−2.5	−16.1	2.3
TSAa1	4.5	2.7	2.0	−23.9	9.1
post_TSAa1	−20.2	−18.8	−18.6	−17.0	−13.5
pre_TSAa2	−3.2	−1.9	−2.1	−18.4	3.4
TSAa2	5.7	3.4	3.0	−20.4	9.1
post_TSAa2	−20.2	−18.8	−18.6	−17.0	−13.5
pre_TSBa1	−2.5	−1.3	−1.3	−17.2	3.8
TSBa1	5.4	3.6	2.9	−23.4	9.9
post_TSBa1	−20.2	−19.1	−18.6	−10.5	−15.5
pre_TSBa2	−2.0	−1.0	−0.9	−15.9	3.8
TSBa2	6.5	4.4	3.9	−21.9	10.4
post_TSBa2	−20.2	−18.9	−18.6	−17.0	−13.5
pre_TSCa1	−2.2	−0.9	−1.0	−18.5	4.5
TSCa1	5.1	3.1	2.6	−21.5	9.0
post_TSCa1	−20.7	−19.6	−19.2	−14.1	−15.0
PI+H_2O	−15.8	−16.0	−15.6	6.0	−17.4

[a] Values relative to the bimolecular reactants are given in kcal·mol^{-1}, except for $\Delta S°$ values that are given in cal·mol^{-1}·K^{-1}.

Dynamical Calculations. The dynamical calculations were carried out using canonical variational transition-state theory with multidimensional tunneling (CVT/MT) contributions.[33]

TABLE 2: Classical Potential Energy (ΔV), Adiabatic Potential Energy (ΔV_a^G), Enthalpy ($\Delta H°$ (298 K)), Entropy ($\Delta S°$ (298 K, 1 M)), and Free Energy ($\Delta G°$ (298 K, 1 M)) for the Reaction R2[a]

structure	ΔV	ΔV_a^G	$\Delta H°$	$\Delta S°$	$\Delta G°$
pre_TSAb1	−3.1	−2.0	−2.0	−16.6	3.0
TSAb1	4.7	3.0	2.2	−24.3	9.5
post_TSAb1	−19.8	−19.0	−18.7	−15.4	−14.1
pre_TSAc1	−2.5	−1.1	−1.2	−17.6	4.0
TSAc1	5.3	3.4	2.7	−23.4	9.7
post_TSAc1	−19.8	−19.3	−18.8	−12.3	−15.1
pre_TSAc2	−3.5	−2.6	−2.5	−16.1	2.3
TSAc2	5.4	3.4	2.8	−21.9	9.3
post_TSAc2	−19.7	−19.1	−18.6	−16.5	−13.7
pre_TSBb1	−2.1	−1.0	−1.0	−17.0	4.1
TSBb1	5.2	3.4	2.7	−23.1	9.6
post_TSBb1	−19.4	−18.5	−18.2	−16.5	−13.3
pre_TSBb2	−2.5	−1.3	−1.3	−17.2	3.8
TSBb2	5.8	4.0	3.4	−22.1	10.0
post_TSBb2	−19.9	−19.6	−19.0	−11.0	−15.7
pre_TSBc1	−1.3	−0.4	−0.2	−13.5	3.8
TSBc1	6.1	4.2	3.5	−23.2	10.4
post_TSBc1	−19.8	−19.3	−18.8	−12.3	−15.1
pre_TSBc2	−2.3	−0.8	−1.1	−20.5	5.1
TSBc2	6.6	4.9	4.1	−25.0	11.5
post_TSBc2	−19.8	−19.3	−18.8	−12.3	−15.1
PIIA + H_2O	−15.6	−16.3	−15.9	4.5	−17.3
pre_TSCb1	−2.5	−1.2	−1.3	−19.7	4.6
TSCb1	5.0	3.3	2.5	−24.6	9.8
post_TSCb1	−19.8	−19.2	−18.7	−13.9	−14.6
pre_TSCc1	−2.5	−1.3	−1.4	−18.9	4.2
TSCc1	4.7	3.1	2.3	−24.5	9.6
post_TSCc1	−20.1	−19.1	−18.9	−17.6	−13.6
PIIB + H_2O	−14.3	−14.9	−14.6	3.9	−15.7

[a] Values relative to the bimolecular reactants are given in kcal·mol^{-1}, except for $\Delta S°$ values that are given in cal·mol^{-1}·K^{-1}.

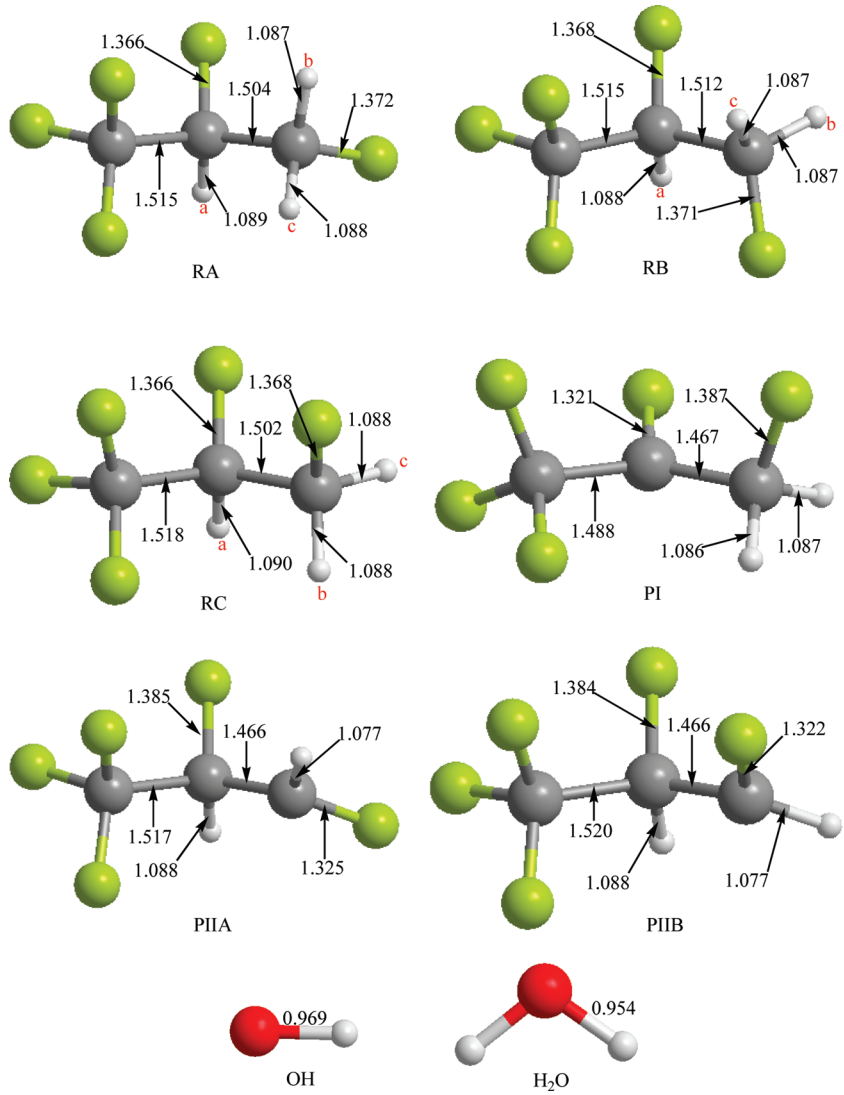

Figure 1. mPW1B95−41.0/6-31+G(d,p) geometries for reactants and products. Distances are given in Ångstroms.

In the present study, tunneling contributions were included using both the small-curvature tunneling (SCT) and the zero-curvature tunneling (ZCT) approximations.[33]

The minimum energy paths (MEPs) in isoinertial mass-scaled Cartesian coordinates[34] were computed by the Page−McIver algorithm[35] with a gradient step-size of 0.005 bohr and with the Hessian matrix being recalculated every 10 steps. The arc length (s) along each MEP was calculated. $s = 0$ is assigned to the transition state structure of the hydrogen abstraction region. Negative or positive values of s correspond to the reactants and products sides, respectively, of the hydrogen abstraction.

Along the MEPs, some of the lowest generalized normal-modes frequencies became imaginary. The zero-order interpolated variational transition-state theory for frequencies (IVTST0FREQ) algorithm[33] was used to correct them.

The spin−orbit coupling is included in the calculation of the electronic partition function of the OH radical by taking into account the excited state $^2\pi_{1/2}$ (140 cm^{-1}).

All the direct dynamics calculations were carried out using PolyRate 9.4.3 and GaussRate 9.4 computer programs.[36,37]

Results and Discussion

Electronic Structure Results. Fourteen independent paths have been found for both reactions R1 and R2. The energies of all those pathways are collected in Tables 1 and 2.

The studied HFC (CF_3CHFCH_2F) exists as three nonequivalent conformers labeled in this work as RA, RB, and RC. The structures of these conformers as well as some selected geometrical parameters are shown in Figure 1. The hydrogens on these conformers are labeled as "a" (the CHF group hydrogen), "b", and "c" (the ones associated to the CH_2F group). Figure 1 also collects the three different final products (PI, PIIA, PIIB), the hydroxyl radical, and the water molecule structures with some selected geometrical parameters.

Three transition state structures (TSs) were located for the interconversion of the three conformers. The barriers (Tables 1 and 2) are low enough to assume a Boltzmann population of the conformers within the range of temperatures considered in this paper. Their structures are shown in Figure S1 of the Supporting Information.

Figure 2 collects the 14 TSs located on the mPW1B95−41.0/6-31+G(d,p) potential energy surfaces (PESs), showing the most interesting geometrical parameters. The notation employed for these structures is as follows:

(1) All names begin with "TS" indicating that those geometries correspond to transition state structures.

(2) A capital letter following "TS" identifies the conformer that undergoes the abstraction process. That is, all the structures with a name beginning with TSA are associated with the RA conformer. The ones whose names begin with TSB are

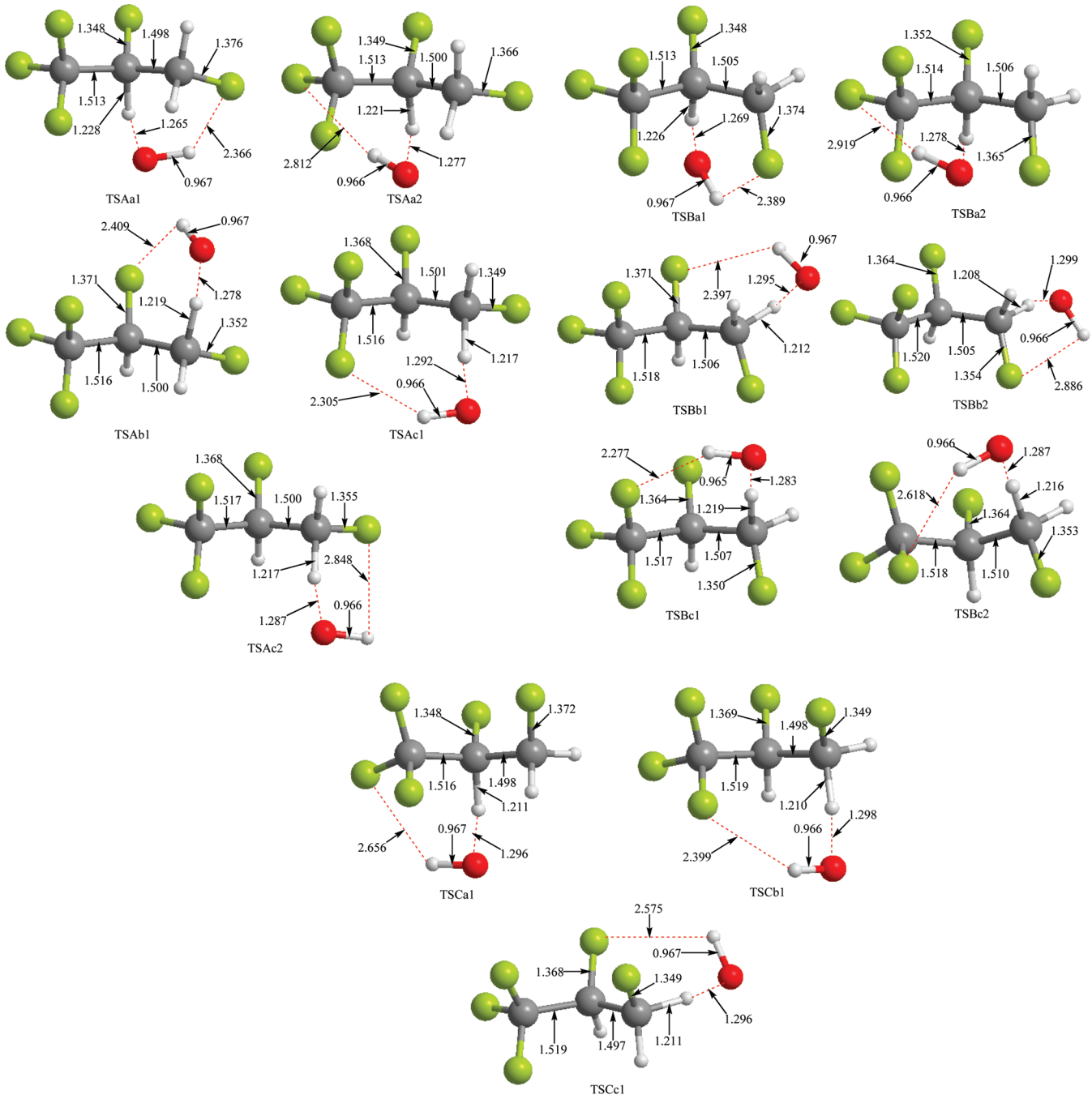

Figure 2. mPW1B95−41.0/6-31+G(d,p) geometries for transition state structures. Distances are given in Ångstroms.

associated with the RB conformer, and the ones whose names begin with TSC are associated with RC.

(3) After the capital letter, a lower-case letter is used for indicating the hydrogen atom that is being abstracted: "a" (R1 reaction), "b" (R2 reaction), or "c" (R2 reaction) as denoted in Figure 1.

(4) Finally, a number is used for differentiating transition state structures associated to the same conformer and identical hydrogen being abstracted.

Thus, TSAa1 means that this structure is a transition state structure for the abstraction of the hydrogen "a" of conformer A, and TSBc2 refers to a transition state structure for the abstraction of the hydrogen "c" of conformer B. Number 2 means that it is the second transition state structure involving conformer B and hydrogen "c".

Following the MEPs from the different TSs to the minimum energy valleys, the corresponding pre- and postreactive complexes were located on the PESs. Their structures are shown in Figure S2 of the Supporting Information.

Figure 3 collects the profiles of the different pathways for both reactions R1 and R2.

All the conformers of CF_3CHFCH_2F and all the TSs have C1 symmetry. Since none of the located TSs has equivalent structures that should be counted as different, in all cases the symmetry number (σ) associated to those TSs has a value of 1; that is, each transition state structure represents only one pathway.

Summarizing, there are 14 nonequivalent kinetic pathways: 5 for reaction R1 (denoted as TSX*a*n, where X = A, B, C and

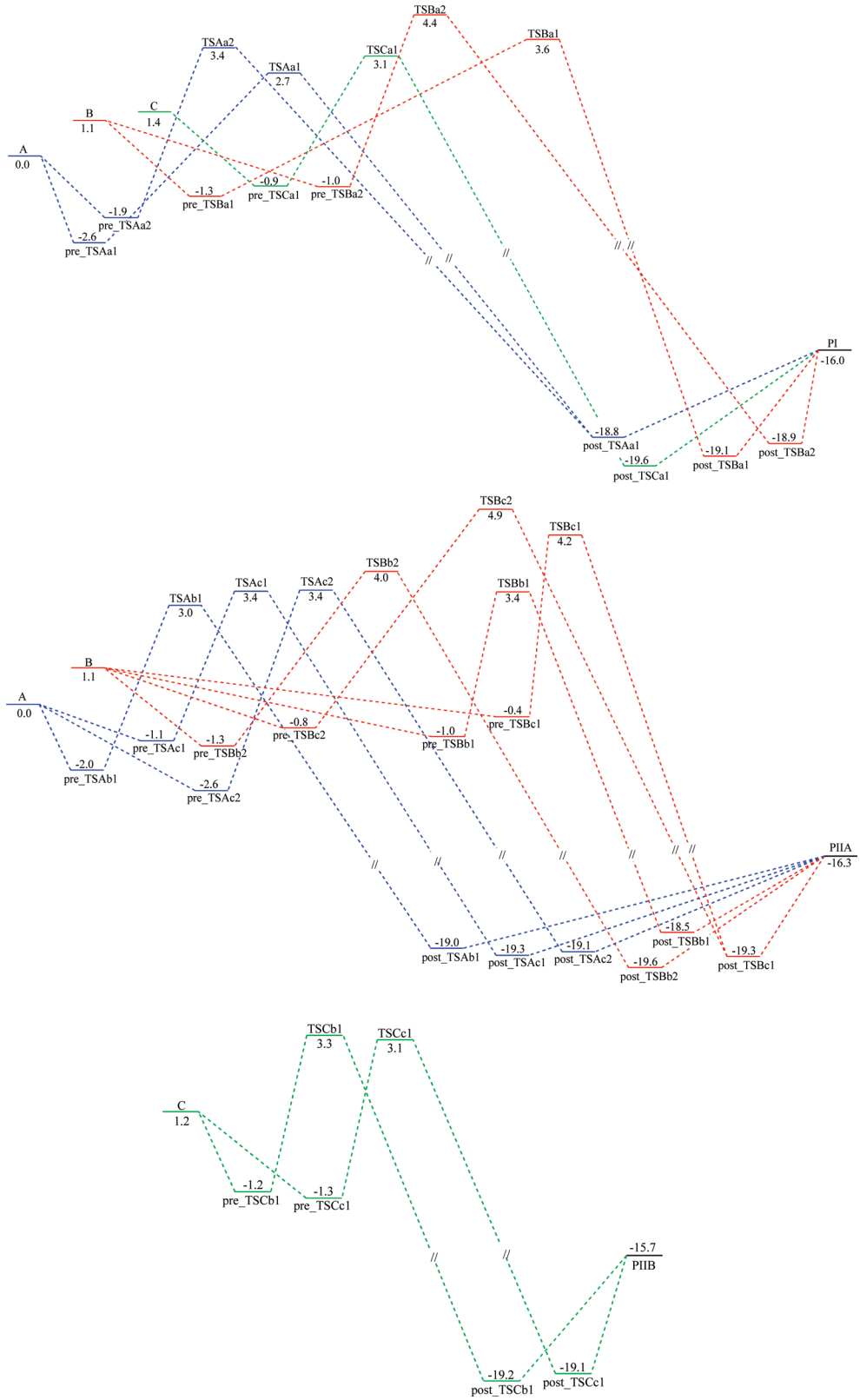

Figure 3. Adiabatic potential energy profiles (kcal·mol^{-1}) for the title reaction: pathways starting from conformers A (blue), B (red), and C (green) are indicated.

$n = 1, 2$) and 9 for reaction R2 (denoted as TSXbn and TSXcn, where X = A, B, C and $n = 1, 2$).

In all cases, the geometries of the transition state structures exhibit four common patterns:

(1) Hammond's postulate. Their geometries resemble their corresponding reactants as expected for strongly exothermic reactions.

(2) Bond forming. The new O−H bonds which are being formed present bond distances ranging from 1.265 (TSAa1) to 1.299 Å (TSBb2). These values are greater than a usual O−H single bond but suggest a very strong O···H interaction.

(3) Bond breaking. The C−H bonds that are being broken show bond distances ranging from 1.208 (TSBb2) to 1.228

Å (TSAa1). These values are greater than a usual C−H single bond but suggest a still very strong C···H interaction.

(4) C−F···H−O interactions. The orientation of the hydroxyl O−H bond is always in a way that allows for the interaction between the hydroxylic hydrogen and one of the fluorine atoms in the CF_3CHFCH_2F molecule. The value of the shortest C−F···H−O distance for every structure is shown in Figure 2. These values range from 2.277 (TSBc1) to 2.919 Å (TSAa2).

Abstraction of hydrogen "a" (reaction R1) leads to a unique final product (PI). However, for reaction R2 two different product conformations exist, depending on the conformer from which the hydrogen is being abstracted: PIIA coming from conformers A and B, and PIIB obtained from conformer C.

Dynamical Results. Based on our previous experience,[27,38] we have considered in the present study the overall flux of the CF_3CHFCH_2F + OH reaction as solely determined by the H-abstraction bottlenecks; that is, we neglected the influence of the loose TSs corresponding to the prereactive formation and postreactive dissociation. This is consistent with the significant energy barriers (over reactants) associated with the hydrogen abstraction bottlenecks that appear for all the channels.

In all the 14 pathways, important variational effects appear (see Tables 3 and S2−S14). The positions corresponding to the adiabatic potential energy maximum, $s(V^{AG})$, and the temperature-dependent dynamical bottleneck, $s_*(T)$, along each MEP are given in Table 3. In all cases the adiabatic potential energy maxima and the dynamical bottlenecks are located on the reactant side of the MEPs. It has to be emphasized that all those reaction channels give significant contributions to the global reaction rate (see Tables S2−S14).

The global rate constants (k_{glob}) for the title reaction, as calculated using TST and CVT theories at different temperatures, are collected in Table 4. This table also contains the corresponding global rate constants obtained when only one of the conformers is considered ($k_{glob,A}$, $k_{glob,B}$, $k_{glob,C}$). These rate constants were computed according to the following equations,

$$k_{glob} = w_A \times (k_{Aa1} + k_{Aa2} + k_{Ab1} + k_{Ac1} + k_{Ac2}) + w_B \times (k_{Ba1} + k_{Ba2} + k_{Bb1} + k_{Bb2} + k_{Bc1} + k_{Bc2}) + w_C \times (k_{Ca1} + k_{Cb1} + k_{Cc1}) = k_{glob,A} + k_{glob,B} + k_{glob,C} \quad (1)$$

$$k_{glob,A} = w_A \times (k_{Aa1} + k_{Aa2} + k_{Ab1} + k_{Ac1} + k_{Ac2}) \quad (2)$$

$$k_{glob,B} = w_B \times (k_{Ba1} + k_{Ba2} + k_{Bb1} + k_{Bb2} + k_{Bc1} + k_{Bc2}) \quad (3)$$

$$k_{glob,C} = w_C \times (k_{Ca1} + k_{Cb1} + k_{Cc1}) \quad (4)$$

In these equations, w_X represents the population (normalized to 1) of the conformer X which can be easily computed from the equilibrium constants between the conformers (Table S15).

The computed CVT/SCT rate constants are at all temperatures somewhat smaller (less than 1 order of magnitude) than the corresponding ones measured by Ravishankara and co-workers[7] (see Table 4). At first sight, it could be considered that the agreement theory-experiment is modest, especially when one compares with our own previous results where this methodology was applied to the study $CF_3CH_2CH_3$ + OH reaction.[27] A deeper analysis shows, however, that present theoretical predictions lay within the chemical accuracy limits for energies (±1 kcal/mol). Let us suppose that discrepancies came only from Gibbs free energies differences, that is, the errors associated to other factors like tunneling are considered to be negligible. Then, it is straightforward to compute the error on the Gibbs free energy barrier by means of the Eyring equation.[33] When Ravishankara and cowokers[7] rate constant values are used, an overestimate of 0.9 kcal/mol for the calculated barrier heights is obtained at all temperatures. At 298 K, the error on the kinetic barrier is 0.8 kcal/mol, when the rate constant value of Nelson and co-workers[6] is used. The chemical accuracy criterion is a very strong condition that is difficult to fulfill even for small molecules and high-level methodologies.[39,40] Since our results do satisfy this criterion, the agreement should be considered reasonably good. Furthermore, computational simulations can provide very valuable information in order to rationalize experiments even when this limit is not fulfilled.[40]

Arrhenius plots of the global rate constants are shown in Figure 4. This figure also shows the Arrhenius plots for the components associated to the three conformers. In Figure S3 the Arrhenius plots of the rate constants, corresponding to the 14 individual nonequivalent pathways, are included. The global rate constants slightly deviate from a straight line when all the calculated temperatures are considered. However, within the experimental range of temperatures (238−374 K) the system shows a perfect linear Arrhenius behavior. Using those values we have obtained:

TABLE 3: Values (in bohr) of $s(V^{AG})$ in the First Row and of $s_*(T)$ in the Rest of Rows for the Different Pathways at Different Temperatures (s = 0 Correspond to Transition State Structures)

T	TSAa1	TSAa2	TSAb1	TSAc1	TSAc2	TSBa1	TSBa2	TSBb1	TSBb2	TSBc1	TSBc2	TSCa1	TSCb1	TSCc1
	−0.34	−0.34	−0.28	−0.29	−0.32	−0.32	−0.33	−0.32	−0.32	−0.29	−0.32	−0.39	−0.33	−0.31
200 K	−0.33	−0.40	−0.26	−0.29	−0.31	−0.32	−0.35	−0.33	−0.29	−0.30	−0.33	−0.47	−0.38	−0.31
238 K	−0.33	−0.41	−0.25	−0.29	−0.31	−0.32	−0.35	−0.34	−0.28	−0.29	−0.33	−0.49	−0.40	−0.31
254 K	−0.33	−0.42	−0.25	−0.28	−0.31	−0.32	−0.35	−0.34	−0.28	−0.29	−0.33	−0.50	−0.41	−0.31
272 K	−0.33	−0.43	−0.24	−0.28	−0.31	−0.32	−0.35	−0.34	−0.27	−0.29	−0.33	−0.51	−0.42	−0.31
297 K	−0.33	−0.44	−0.24	−0.28	−0.31	−0.31	−0.35	−0.35	−0.27	−0.29	−0.34	−0.53	−0.44	−0.31
298 K	−0.33	−0.44	−0.24	−0.28	−0.31	−0.31	−0.35	−0.35	−0.27	−0.29	−0.34	−0.53	−0.44	−0.31
324 K	−0.33	−0.46	−0.23	−0.28	−0.31	−0.31	−0.36	−0.36	−0.26	−0.29	−0.34	−0.54	−0.46	−0.31
348 K	−0.33	−0.47	−0.22	−0.28	−0.31	−0.31	−0.36	−0.37	−0.25	−0.29	−0.34	−0.56	−0.47	−0.31
349 K	−0.33	−0.47	−0.22	−0.28	−0.31	−0.31	−0.36	−0.37	−0.25	−0.29	−0.34	−0.56	−0.47	−0.31
374 K	−0.22	−0.48	−0.19	−0.28	−0.31	−0.31	−0.36	−0.38	−0.25	−0.29	−0.34	−0.57	−0.49	−0.31
400 K	−0.22	−0.50	−0.17	−0.27	−0.31	−0.31	−0.36	−0.40	−0.23	−0.29	−0.34	−0.59	−0.51	−0.31
600 K	−0.20	−0.59	−0.13	−0.26	−0.30	−0.30	−0.38	−0.55	0.06	−0.28	−0.36	−0.68	−0.59	−0.30
800 K	−0.19	−0.66	−0.02	−0.24	−0.15	−0.28	−0.40	−0.63	0.08	−0.28	−0.38	−0.76	−0.63	−0.30

$$k^{\mathrm{CVT/SCT}}(T) = 1.44 \times 10^{-12} \exp[(-1753)/T] \quad \mathrm{cm^3 \cdot molecule^{-1} \cdot s^{-1}}$$

that can be compared with the one by Ravishankara and co-workers:[7]

$$k^{\mathrm{Rav}}_{\mathrm{exp}}(T) = (1.23 \pm 0.18) \times 10^{-12} \exp[(-1250 \pm 40)/T] \quad \mathrm{cm^3 \cdot molecule^{-1} \cdot s^{-1}}$$

The predicted activation energy from our calculations is 3.5 kcal/mol, which represents a good agreement with the value obtained by Ravishankara and co-workers (2.5 kcal/mol).

At all temperatures, the contribution associated to conformer A is the most important one but it decreases as the temperature grows (from 76.8% at 200 K to 46.8% at 800 K). The contribution of conformer B increases with temperature from 10.6% (200 K) to 36.2% (800 K). At 200 K it is the less important contribution, but at 800 K it becomes almost as important as the conformer A contribution. The contribution from conformer C is the less important one at all temperatures but at 200 K, where it is slightly greater than that from conformer B. The variation of this latter contribution with temperature is not as important as the ones from conformers A and B. It takes values between 12.6% and 17.4% of the global rate constant. These results clearly show that the three conform-

TABLE 4: Population of Each Conformer, TST, CVT, and CVT/SCT Rate Constants, CHF Contribution (%) (Reaction R1) and CH_2F Contribution (%) (Reaction R2) to the Global Rate Constants, Contributions (%) of Each Conformer, and Global Experimental Rate Constants for the Title Reaction at some Selected Temperatures[a]

T	rot.	pop.	TST	CVT	CVT/SCT	CHF cont.	CH_2F cont.	rot. cont.	exp.
200	A	0.91	3.02(−16)	5.57(−17)	2.18(−16)	38.25	38.57	76.82	
	B	0.07	6.19(−17)	9.66(−18)	2.99(−17)	2.76	7.81	10.57	
	C	0.02	1.52(−16)	1.37(−17)	3.57(−17)	3.32	9.28	12.61	
	global	1.00	5.16(−16)	7.91(−17)	2.83(−16)	44.33	55.67	100.00	
238	A	0.86	1.03(−15)	2.57(−16)	6.68(−16)	35.28	35.69	70.98	
	B	0.11	2.65(−16)	6.13(−17)	1.37(−16)	3.83	10.69	14.52	
	C	0.03	5.41(−16)	7.19(−17)	1.37(−16)	4.66	9.84	14.50	
	global	1.00	1.84(−15)	3.90(−16)	9.41(−16)	43.78	56.22	100.00	6.3(−15)
254	A	0.84	1.57(−15)	4.29(−16)	9.92(−16)	34.12	34.76	68.88	
	B	0.12	4.34(−16)	1.14(−16)	2.31(−16)	4.26	11.78	16.05	
	C	0.04	8.31(−16)	1.25(−16)	2.17(−16)	5.14	9.93	15.08	
	global	1.00	2.84(−15)	6.69(−16)	1.44(−15)	43.53	56.47	100.00	9.4(−15)
272	A	0.82	2.40(−15)	7.18(−16)	1.49(−15)	33.03	33.80	66.82	
	B	0.14	7.10(−16)	2.13(−16)	3.92(−16)	4.73	12.88	17.61	
	C	0.04	1.27(−15)	2.17(−16)	3.47(−16)	5.62	9.95	15.57	
	global	1.00	4.38(−15)	1.15(−15)	2.23(−15)	43.37	56.63	100.00	1.22(−14)
298	A	0.79	4.09(−15)	1.37(−15)	2.50(−15)	31.68	32.57	64.26	
	B	0.16	1.32(−15)	4.61(−16)	7.67(−16)	5.35	14.35	19.70	
	C	0.05	2.16(−15)	4.30(−16)	6.25(−16)	6.16	9.88	16.04	
	global	1.00	7.57(−15)	2.26(−15)	3.89(−15)	43.19	56.81	100.00	1.81(−14) 1.48(−14)
324	A	0.76	6.49(−15)	2.38(−15)	3.93(−15)	30.43	31.60	62.03	
	B	0.18	2.25(−15)	8.92(−16)	1.37(−15)	5.94	15.64	21.59	
	C	0.06	3.41(−15)	7.70(−16)	1.04(−15)	6.60	9.78	16.38	
	global	1.00	1.22(−14)	4.04(−15)	6.34(−15)	42.98	57.02	100.00	2.50(−14)
349	A	0.74	9.59(−15)	3.79(−15)	5.82(−15)	29.51	30.82	60.33	
	B	0.20	3.53(−15)	1.55(−15)	2.23(−15)	6.48	16.64	23.11	
	C	0.07	5.00(−15)	1.25(−15)	1.60(−15)	6.93	9.63	16.56	
	global	1.00	1.81(−14)	6.59(−15)	9.64(−15)	42.91	57.09	100.00	3.39(−14)
374	A	0.71	1.36(−14)	5.68(−15)	7.70(−15)	27.40	29.73	57.13	
	B	0.21	5.26(−15)	2.52(−15)	3.44(−15)	7.28	18.21	25.49	
	C	0.07	7.04(−15)	1.92(−15)	2.34(−15)	7.50	9.88	17.39	
	global	1.00	2.59(−14)	1.01(−14)	1.35(−14)	42.18	57.82	100.00	4.58(−14)
600	A	0.58	1.12(−13)	5.96(−14)	6.36(−14)	23.74	25.87	49.61	
	B	0.30	5.62(−14)	3.96(−14)	4.23(−14)	10.94	22.09	33.03	
	C	0.11	5.40(−14)	2.14(−14)	2.23(−14)	8.72	8.63	17.36	
	global	1.00	2.22(−13)	1.21(−13)	1.28(−13)	43.40	56.60	100.00	
800	A	0.52	3.47(−13)	1.93(−13)	1.96(−13)	23.13	23.62	46.75	
	B	0.35	1.94(−13)	1.46(−13)	1.52(−13)	12.91	23.32	36.23	
	C	0.13	1.60(−13)	6.98(−14)	7.12(−14)	8.99	8.04	17.02	
	global	1.00	7.01(−13)	4.08(−13)	4.18(−13)	45.03	54.97	100.00	

[a] Rate constants are given in $\mathrm{cm^3 \cdot molecule^{-1} \cdot s^{-1}}$. Power of 10 in parentheses.

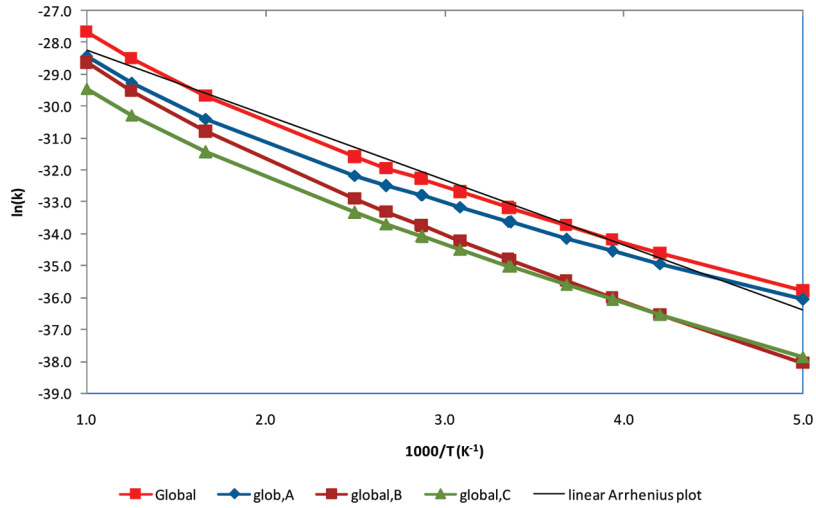

Figure 4. Arrhenius plots for the global rate constants ($cm^3 \cdot molecule^{-1} \cdot s^{-1}$). The Arrhenius plots for the conformer contributions ($k_{glob,A}$, $k_{glob,B}$, $k_{glob,C}$) are also included.

ers play an important role in the title reaction, and, as a consequence, all the corresponding pathways have to be considered to get a satisfactory mechanistic picture.

As mentioned above (Introduction section), there are two possible reactions, labeled as R1 and R2, associated with the title reaction. Equation R1 results from abstraction of the hydrogen at CHF group. Equation R2 results from abstraction of any of the hydrogens at CH_2F group. The contribution of these groups to the rate constant can be easily estimated as

$$k_{R1} = \sum_{X\in(A,B,C)} \sum_{n=1,2} w_X k_{TSXan} \quad (5)$$

$$k_{R2} = \left[\sum_{X\in(A,B,C)} \sum_{n=1,2} w_X k_{TSXbn}\right] + \left[\sum_{X\in(A,B,C)} \sum_{n=1,2} w_X k_{TSXcn}\right] \quad (6)$$

The present results predict that the greatest contribution come from the CH_2F group. This contribution increases from 55.7% (200 K) to 57.8% (374 K), and then decreases to 55.0% (800 K). Consequently, the opposite pattern is found for the CHF group contribution. These contributions are nearly invariant; they change only about 3% of the global rate constant over a range of temperatures that covers 600 K.

Ravishankara and co-workers[7] used the SAR by Tokuhashi and co-workers[9] for estimating the contribution from CH_2F and CHF groups at 298 K. They obtained a value of $k(298\ K) = 1.05 \times 10^{-14}\ cm^3 \cdot molecule^{-1} \cdot s^{-1}$, with contributions of about 50% from both groups.[7] We recomputed those values (taking into account the number of hydrogen atoms that can be abstracted for each reaction) and obtained $k(298\ K) = 1.57 \times 10^{-14}\ cm^3 \cdot molecule^{-1} \cdot s^{-1}$ (which is exactly the value that appears in Table 6 of the original work by Tokuhashi and co-workers)[9] with contributions of 35% (CHF group) and 65% (CH_2F group) to the global rate constant. The global rate constant almost matches the experimental value obtained by Nelson and co-workers[6] (within 6%) and is in excellent agreement with the one by Ravishankara and co-workers (within 14%). On the other hand, the contribution from the CH_2F group is slightly overestimated when comparing with our computational predictions (43% from the CHF group and 57% from the CH_2F group). We can conclude that Tokuhashi and co-workers' SAR does a pretty good job on this reaction, although it fails to treat the similar reaction $CF_3CH_2CH_3$ + OH.[27]

Ravishankara and co-workers[7] also used the SAR developed by DeMore[4] and obtained an almost equal contribution from both groups. With this SAR, we obtained a value of $k(298\ K) = 1.26 \times 10^{-14}\ cm^3 \cdot molecule^{-1} \cdot s^{-1}$, with contributions of 41% (CHF group) and 59% (CH_2F group). The global rate constant agrees rather well with the value reported by Nelson and co-workers[6] (within 15%), and it can be considered compatible with the value reported by Ravishankara and co-workers (within 31%). The above group contributions to the global rate constant are in excellent agreement with the ones theoretically predicted in the present work. Once more, for the reaction with $CF_3CH_2CH_3$ this SAR behaves in a different way. It produces a good agreement with the experimental values of the global rate constants but gives a poor agreement with the contributions from CH_2 and CH_3 groups.[27]

We also used a new improved version of this SAR[5] and got a value of $k(298\ K) = 2.39 \times 10^{-14}\ cm^3 \cdot molecule^{-1} \cdot s^{-1}$, with contributions of 41% (CHF group) and 59% (CH_2F group). This new version provides a reasonably good agreement with the experimental value reported by Ravishankara and co-workers[7] (within 32%), while the agreement with the values reported by Nelson and co-workers[6] (within 62%) clearly deteriorates. The excellent agreement with our predicted theoretical contributions is preserved. Previously,[27] we reported that this SAR, when applied to the $CF_3CH_2CH_3$ + OH reaction, improved both the value of the global rate constant and the predicted contributions from the groups (although the agreement with the computed values resulted still poor). Therefore, the behavior of this SAR for the $CF_3CH_2CH_3$ + OH and CF_3CHFCH_2F + OH reactions is different.

Tunneling contributions (see transmission coefficients in Tables S2−S14) are negligible only at higher temperatures (600 K and over). At lower temperatures (200−272 K), tunneling contributions are important, multiplying the CVT rate constant by a factor of roughly 2−4. However, they are not as important as expected for a hydrogen transfer between two heavy atoms. Like in the case of the $CF_3CH_2CH_3$ + OH reaction, the adiabatic curves are rather wide (Figure S4), which makes tunneling contributions smaller than expected.

As mentioned above, an article dealing with this reaction has recently been published by Gao et al.[28] These authors used dual level kinetics calculations (G3(MP2)//BB1K/6-31+G(d,p)) to

obtain the improved canonical variational transition-state (ICVT) theory rate constant with tunneling effects estimated at the SCT level. Gao et al. only included the conformer A in their study and used the following kinetic equation:

$$k_{\mathrm{glob,A}}^{\mathrm{Gao}} = (k_{\mathrm{Aa1}} + k_{\mathrm{Ab1}} + k_{\mathrm{Ac1}} + k_{\mathrm{Ac2}}) \qquad (7)$$

It should be noted that in the original work by Gao et al., k_{Aa1} corresponds to k_{2a}, k_{Ab1} corresponds to k_{2c}, k_{Ac1} corresponds to $k_{2b-\alpha}$, and k_{Ac2} corresponds to $k_{2b-\beta}$. On the other hand, k_{Aa2} is missing in eq 7 because the corresponding pathway was not located on the BB1K/6-31+G(d,p) PES by Gao et al. However, according to our calculations, the contribution of this last channel increases with temperature from 4.7% (200 K) to 14.1% (800 K) and becomes the most important pathway at temperatures higher than 600 K (see Tables S2−S14). In addition, Gao et al. implicitly assumed that eqs 3 and 4 can both be discarded; that is, global contribution from conformers B and C is negligible. However, in the present work it is shown that such contribution grows as the temperature increases, ranging from 23.2% (200 K) to 53.3% (800 K) of the global rate constant. Consequently, conformers B and C should be considered in order to get a realistic picture of the mechanism through which the title reaction proceeds.

Conclusions

We have computed and analyzed the rate constants for the hydrogen abstraction reaction between CF_3CHFCH_2F and OH radical over a range of temperatures from 200 to 800 K. CVT/SCT direct dynamics approach, based on a hybrid meta-GGA DFT functional parametrized in accordance with a specific reaction parameter (SRP) approach, was the method chosen. The functional used was adjusted (in a previous work by Albu and Swaminathan) using the CH_3F + OH hydrogen abstraction as a model reaction.

Fourteen different reaction channels have been explored, all of them with significant contributions to the global rate constants. Among the three CF_3CHFCH_2F conformers, the most stable one (RA) makes the greatest contribution to the global rate constant at all the temperatures considered. However, the contributions of the two remaining conformers are not negligible at any of the analyzed temperatures, and at higher temperatures their joint contribution is greater than the one from conformer A. For this reason, the previous theoretical work by Gao et al., who only considered conformer A in their calculations, does not provide a complete picture of the reaction mechanism.

Of the two reactive groups present in the CF_3CHFCH_2F molecule, the CH_2F group is the most reactive one at every considered temperature. Its contributions represent between 55% and 58% of the global rate constant.

We studied the viability of Albu and Swaminathan approach with the $CF_3CH_2CH_3$ + OH reaction, obtaining a very good agreement. In the present work, the agreement is somewhat worse but still lays within the limits of chemical accuracy (errors of ± 1 kcal/mol on calculated barrier heights). This agreement is good enough as to validate the transferability of the functional by Albu and Swaminathan.

Acknowledgment. We are grateful for financial support from the Spanish Ministerio de Ciencia e Innovación through projects CTQ2008-02403/BQU and CTQ2007-67234-C02-01/BQU, the Generalitat de Catalunya (2009SGR00409), and the Gobierno del Principado de Asturias (IB08-023).

Supporting Information Available: The Supporting Information contains energy values at the stationary points located on the potential energy surfaces, individual rate constants for each individual pathway, contributions of each pathway, group and conformer as a function of temperature, equilibrium constants for the interconversion between the conformers, Cartesian coordinates for all the computed structures, geometries for the transition states structures corresponding to the interconversion of the three conformers, geometries for pre- and postreactive complexes located on the potential energy surfaces, Arrhenius plots of the individual rate constants corresponding to the 14 nonequivalent reaction pathways, and adiabatic ground state potential energy curves for the fourteen nonequivalent reaction pathways. This material is available free of charge via the Internet at http://pubs.acs.org.

References and Notes

(1) (a) *WMO Scientific Assessment of Ozone Depletion 2002: Global ozone research monitoring project no 47*; WMO: Geneva, 2003. (b) Velders, G. J. M.; Falhey, D. W.; Daniel, J. S.; McFarland, M.; Andersen, S. O. *Proc. Natl. Acad. Sci. U.S.A.* **2009**, *106*, 10949.

(2) Atkinson, R. In *Air Pollution, the Automobile, and Public Health*; Watson, A. I.; Bates, R. R.; Kennedy, D., Eds.; National Academic Press: Washington, D.C., 1988; pp. 99−132.

(3) (a) Jeong, K. M.; Kaufman, F. *J. Phys. Chem.* **1982**, *86*, 1808. (b) Schmoltner, A. M.; Talukdar, R. K.; Warren, R. F.; Mellouki, A.; Goldfard, L.; Gierczak, T.; McKeen, S. A.; Ravishankara, A. R. *J. Phys. Chem.* **1993**, *97*, 8976. (c) Takular, R.; Mellouki, A.; Gierczak, T.; Burkholder, J. B.; McKeen, S. A.; Ravishankara, A. R. *J. Phys. Chem.* **1991**, *95*, 5815. (d) Wilson, E. W., Jr.; Jacoby, A. M.; Kukta, S. J.; Gilbert, L. E.; DeMore, W. B. *J. Phys. Chem. A* **2003**, *107*, 9357. (e) Young, C. J.; Hurley, M. D.; Wallington, T. J.; Mabury, S. A. *Chem. Phys. Lett.* **2009**, *473*, 251.

(4) DeMore, W. B. *J. Phys. Chem.* **1996**, *100*, 5813.

(5) DeMore, W. B.; Wilson, E. W., Jr. *J. Phys. Chem. A* **1999**, *103*, 573.

(6) Nelson, D. D., Jr.; Zahniser, M. S.; Kolb, C. E.; Magid, H. *J. Phys. Chem. A* **1995**, *99*, 16301.

(7) Rajakumar, B.; Portmann, R. W.; Burkholder, J. B.; Ravishankara, A. R. *J. Phys. Chem. A* **2006**, *110*, 6724.

(8) (a) Atkinson, R. *Int. J. Chem. Kinet.* **1987**, *19*, 799. (b) Kwok, E. S. C.; Atkinson, R. *Atmos. Environ.* **1995**, *29*, 1685.

(9) Tokuhashi, K.; Nagai, H.; Takahashi, A.; Kaise, M.; Kondo, S.; Sekiya, A.; Takahashi, M.; Gotoh, Y.; Suga, A. *J. Phys. Chem. A* **1999**, *103*, 2664.

(10) Urata, S.; Takada, A.; Uchimaru, T.; Chandra, A. K. *Chem. Phys. Lett.* **2003**, *368*, 215.

(11) Percival, C. J.; Marston, G.; Wayne, R. P. *Atmos. Environ.* **1995**, *29*, 305.

(12) Dhanya, S.; Saini, R. D. *Int. J. Chem. Kinet.* **1997**, *29*, 187.

(13) Jeong, K. M.; Kaufman, F. *J. Phys. Chem.* **1982**, *86*, 1816.

(14) (a) Cohen, N.; Benson, S. W. *J. Phys. Chem.* **1987**, *91*, 162. (b) Cohen, N.; Benson, S. W. *J. Phys. Chem.* **1987**, *91*, 171.

(15) Schwartz, M.; Marshall, P.; Berry, R. J.; Ehlers, C. J.; Petersson, G. A. *J. Phys. Chem. A* **1998**, *102*, 10074.

(16) (a) Korchowiec, J.; Kawahara, S.-I.; Matsumura, K.; Uchimara, T.; Surgie, M. *J. Phys. Chem. A* **1999**, *103*, 3548. (b) Korchowiec, J. *J. Phys. Org. Chem.* **2002**, *15*, 524.

(17) Louis, F.; Gonzalez, C. A.; Huie, R. E.; Kurylo, M. J. *J. Phys. Chem. A* **2000**, *104*, 8773.

(18) Fontana, G.; Causà, M.; Gianotti, V.; Marchionni, G. *J. Fluor. Chem.* **2001**, *109*, 113.

(19) Sun, H.; He, H.; Gong, H.; Pan, X.; Li, Z.; Wang, R. *Chem. Phys.* **2006**, *327*, 91.

(20) Zhang, M.; Lin, Z.; Song, C. *J. Chem. Phys.* **2007**, *126*, 034307.

(21) (a) Espinosa-García, J.; Coitiño, E. L.; González-Lafont, A.; Lluch, J. M. *J. Phys. Chem. A* **1998**, *102*, 10715. (b) González-Lafont, A.; Lluch, J. M.; Espinosa-García, J. *J. Phys. Chem. A* **2001**, *105*, 10553. (c) Espinosa-García, J. *J. Phys. Chem. A* **2002**, *106*, 5686.

(22) Lien, P.-Y.; You, R.-M.; Hu, W.-P. *J. Phys. Chem. A* **2001**, *105*, 2391.

(23) Sekušak, S.; Sabljić, A. *J. Phys. Chem. A* **2001**, *105*, 1968.

(24) (a) Albu, T. V.; Swaminathan, S. *J. Phys. Chem. A* **2006**, *110*, 7663. (b) Albu, T. V.; Swaminathan, S. *Theor. Chem. Acc.* **2007**, *117*, 383.

(25) Zhang, L.; Li, S. *J. Mol. Struct.: THEOCHEM* **2009**, *869*, 6.

(26) (a) Wang, Y.; Liu, J.-Y.; Yang, L.; Zhao, X.-L.; Ji, Y.-M.; Li, Z.-S. *J. Phys. Chem. A* **2007**, *111*, 7761. (b) Gao, H.; Wang, Y.; Liu, J.-Y.;

Yang, L.; Li, Z.-S.; Sun, C.-C. *J. Phys. Chem. A* **2008**, *112*, 4176. (c) Gao, H.; Wang, Y.; Wang, Q.; Liu, J.-Y.; Sun, C.-C. *Theor. Chem. Acc.* **2009**, *124*, 59.

(27) Gonzalez-Lafont, A.; Lluch, J. M.; Varela-Álvarez, A.; Sordo, J. A. *J. Phys. Chem. B* **2008**, *112*, 328.

(28) Gao, H.; Liu, J.-Y.; Sun, C.-C. *J. Chem. Phys.* **2009**, *130*, 224301.

(29) Frisch, M. J.; Trucks, G. W.; Schlegel, H. B.; Scuseria, G. E.; Robb, M. A.; Cheeseman, J. R.; Montgomery, J. A., Jr.; Vreven, T.; Kudin, K. N.; Burant, J. C.; Millam, J. M.; Iyengar, S. S.; Tomasi, J.; Barone, V.; Mennucci, B.; Cossi, M.; Scalmani, G.; Rega, N.; Petersson, G. A.; Nakatsuji, H.; Hada, M.; Ehara, M.; Toyota, K.; Fukuda, R.; Hasegawa, J.; Ishida, M.; Nakajima, T.; Honda, Y.; Kitao, O.; Nakai, H.; Klene, M.; Li, X.; Knox, J. E.; Hratchian, H. P.; Cross, J. B.; Bakken, V.; Adamo, C.; Jaramillo, J.; Gomperts, R.; Stratmann, R. E.; Yazyev, O.; Austin, A. J.; Cammi, R.; Pomelli, C.; Ochterski, J. W.; Ayala, P. Y.; Morokuma, K.; Voth, G. A.; Salvador, P.; Dannenberg, J. J.; Zakrzewski, V. G.; Dapprich, S.; Daniels, A. D.; Strain, M. C.; Farkas, O.; Malick, D. K.; Rabuck, A. D.; Raghavachari, K.; Foresman, J. B.; Ortiz, J. V.; Cui, Q.; Baboul, A. G.; Clifford, S.; Cioslowski, J.; Stefanov, B. B.; Liu, G.; Liashenko, A.; Piskorz, P.; Komaromi, I.; Martin, R. L.; Fox, D. J.; Keith, T.; Al-Laham, M. A.; Peng, C. Y.; Nanayakkara, A.; Challacombe, M.; Gill, P. M. W.; Johnson, B.; Chen, W.; Wong, M. W.; Gonzalez, C.; Pople, J. A. *Gaussian 03, Revision C.01*; Gaussian, Inc., Wallingford, CT, 2004.

(30) Adamo, C.; Barone, V. *J. Chem. Phys.* **1998**, *108*, 664.

(31) Becke, A. D. *J. Chem. Phys.* **1996**, *104*, 1040.

(32) Perdew, J. P.; Kurth, S. In *A Primer in Density Functional Theory*; Fiolhais, C.; Nogueira, F.; Marques, M., Eds.; Springer-Verlag: Berlin, 2003.

(33) Fernández-Ramos, A.; Miller, J. A.; Klippenstein, S. J.; Truhlar, D. G. *Chem. Rev.* **2006**, *106*, 4518, and references therein.

(34) Fukui, K. *Acc. Chem. Res.* **1981**, *14*, 363.

(35) Page, M.; McIver, J. W., Jr. *J. Chem. Phys.* **1988**, *88*, 922.

(36) Corchado, J. C.; Chuang, Y.-Y.; Fast, P. L.; Hu, W.-P.; Liu, Y.-P.; Lynch, G. C.; Nguyen, K. A.; Jackels, C. F.; Fernandez Ramos, A.; Ellingson, B. A.; Lynch, B. J.; Melissas, V. S.; Villà, J.; Rossi, I.; Coitiño, E.L.; Pu, J.; Albu, T. V.; Steckler, R.; Garrett, B. C.; Isaacson, A. D.; Truhlar, D. G. *PolyRate*, version 9.4.3; University of Minnesota: Minneapolis, MN, 2007. http://comp.chem.umn.edu/polyrate.

(37) Corchado, J. C.; Chuang, Y.-Y.; Coitiño, E. L.; Truhlar, D. G. *GaussRate*, version 9.4; University of Minnesota: Minneapolis, MN, 2007. http://comp.chem.umn.edu/gaussrate.

(38) Varela-Álvarez, A.; Rayón, V. M.; Redondo, P.; Barrientos, C.; Sordo, J. A. *J. Chem. Phys.* **2009**, *131*, 144309.

(39) (a) Feller, D.; Sordo, J. A. *J. Chem. Phys.* **2000**, *112*, 5604. (b) Feller, D.; Sordo, J. A. *J. Chem. Phys.* **2000**, *113*, 485. (c) Sordo, J A. *J. Chem. Phys.* **2001**, *114*, 1974. (d) Feller, D.; Peterson, K. A.; de Jong, W. A.; Dixon, D. A. *J. Chem. Phys.* **2003**, *118*, 3510. (e) Feller, D.; Peterson, K. A.; Crawford, T. D. *J. Chem. Phys.* **2006**, *124*, 054107.

(40) Varela-Álvarez, A.; Markovic, D.; Vogel, P.; Sordo, J. A. *J. Am. Chem. Soc.* **2009**, *131*, 9547.

JP909675U